The Effect of Structural Material Parameters on the Operational Characteristic of Traction Drives for EV Applications

N. Leuning[1], D. Ukwungwu[1], M. Nell[1], F. Pauli[1], S. Steentjes[2], and K. Hameyer[1]

[1]Institute of Electrical Machines (IEM), RWTH Aachen University, Aachen 52062, Germany
[2]Hilti Entwicklungsgesellschaft mbH, Kaufering 86916, Germany

In this article, the effect of structural material parameters of nongrain-oriented (NO) electrical steel on the driving cycle losses and torque–speed characteristics of electrical traction drives for electric vehicle (EV) applications is studied. The operating point distribution in different driving cycles affects the iron losses and magnetization behavior. As a result, the ideal material choice not only depends on the machine design and topology but also on the application requirements. Structural material parameters of electrical steel, that is, alloying, sheet thickness, grain size, and crystallographic texture, are measures to modulate the magnetic properties. Their effect on iron-loss components is studied for seven industrial NO electrical steel grades. Two traction drives and four driving cycles are evaluated with respect to the structural material parameters as application examples.

***Index Terms*— Automotive drive cycle, ferromagnetic material choice, loss modeling, structural material parameter electrical steel.**

I. Introduction

NONGRAIN-ORIENTED (NO) electrical steels are used to guide the magnetic flux in rotating electrical machines. The magnetic flux inside the air gap generates the torque. The ideal NO material is easy to magnetize and has low-frequency-dependent iron losses. However, due to the nonlinear magnetization curve and frequency dependence of the magnetic properties, for example, required magnetic field and loss, the optimization of said properties is operating point dependent. During the design process of electrical machines, the material choice of the NO electrical steel is generally based on standard classifications, supplier datasheets, or standardized magnetic measurements. These sources of information have in common that they rely on discrete excitation conditions. Magnetic properties at 50 and 400 Hz do not reflect speed-variable, that is, frequency-dependent iron losses [1], [2].

As the magnetic properties of NO electrical steels, just like other technological properties of crystalline materials, stem from deviations of the ideal crystal structure, the influences of material parameters on magnetic properties are critical to understand as well as to estimate the magnetic behavior. Furthermore, an improved material design can thereby be enabled. Structural material properties, for example, alloying, sheet thickness, grain size, or crystallographic texture, are measures to design the magnetic properties of NO electrical steel [3]–[5]. According to the domain and loss theories [6]–[8], domain wall movement and hysteresis losses are affected by lattice defects, such as grain boundaries or impurities [9]. These lattice defects act as pinning points for the free domain wall movement. An increased magnetic field is necessary to magnetize the material. Thus, grain size has a dominant effect on the magnetic properties. The alloying with silicon increases the electrical resistivity, in order to decrease the classical Foucault losses. However, due to the lower content of magnetic material, the saturation polarization is decreased. The crystal orientation in different grains, that is, crystallographic texture, affects the isotropy and value of the magnetization due to the distribution of easy and hard magnetization axes relative to the magnetization direction [10]–[12]. Finally, the sheet thickness can significantly decrease the classical Foucault losses, but thin sheets reduce the maximum filling factor due to the higher proportion of insulating coating. Furthermore, such thin sheets are challenging concerning their processing and handling and are generally higher priced.

This article studies the effect of structural material parameters of seven NO materials on the iron-loss components and, subsequently, on the operational characteristics (driving cycle losses and torque–speed characteristics) of electrical traction drives for electric vehicle (EV) applications. Currently, NO materials are chosen mainly based on their magnetic properties, that is, the loss and magnetization characteristics at specific flux density levels and frequencies. These selection criteria are weak and give limited interpolation and extrapolation possibilities due to the missing focus on the underlying relations of the magnetization process. Better understanding of the material properties allows one to tailor the NO materials and the motor design to achieve the best possible motor performance.

II. Experimental Results

A. Materials and Magnetic Measurements

In this article, seven industrial NO materials are characterized in terms of chemical composition by using a spark spectrometer: the mean grain size d_{GS} (line intercept method), crystallographic texture (XRD), electrical resistivity ρ_{el} via measurement according to [13], and sheet thickness d_s is measured with a micrometer screw. An overview on the properties

Manuscript received May 8, 2020; revised June 23, 2020; accepted July 15, 2020. Date of publication July 31, 2020; date of current version January 20, 2021. Corresponding author: N. Leuning (e-mail: nora.leuning@iem.rwth-aachen.de).

Color versions of one or more of the figures in this article are available online at https://ieeexplore.ieee.org.

Digital Object Identifier 10.1109/TMAG.2020.3013322

TABLE I
STRUCTURAL MATERIAL PARAMETERS OF THE STUDIED NO MATERIALS

Material	Silicon in wt.%	d_s in mm	d_{GS} in µm	ρ_{el} in µΩcm	A-parameter in ° [11]
M1	3.6	0.297	82	62	31.7
M2	3.5	0.298	99	54	31.6
M3	3.4	0.483	73	58	32.3
M4	2.6	0.350	67	45	34.8
M5	3.3	0.350	126	51	30.7
M6	3.8	0.199	95	59	32.3
M7	2.9	0.110	78	63	34.1

is given in Table I. The so-called A-parameter is used to quantify the crystallographic texture of electrical steel according to [11]. A represents the distribution of easy magnetization axes of the crystal orientations, relative to the magnetization in the sheet plane of electrical steel. Magnetic measurements are performed from measurements in the quasi-static regime up to 5.000 Hz on a 120 mm × 120 mm single-sheet tester (SST).

B. IM and Permanent-Magnet Synchronous Machine Topology and Vehicle Model

Two motor topologies, an induction machine (IM) and a permanent-magnet synchronous machine (PMSM) for the fully electric drivetrain of EV applications, are simulated via finite-element analysis (FEA) and evaluated with respect to various driving cycles. The results of the parameter identification and FEA are correlated with the structural material parameters and their impact on the operational characteristics is evaluated.

Both IM and PMSM topologies are common in commercial EV applications. The studied IM is a four-pole machine with a squirrel cage, with a maximum speed of 10 000 r/min, and with a continuous power of 40 kW. The outer stator diameter is 175 mm. In the electric drivetrain, two machines are employed to form a dual-motor drive to achieve the specified power output. All required points of operation in the torque–speed map are derived from the driving cycles chosen. The PMSM studied also has four pole pairs and a maximum speed of 6000 r/min, a continuous power of 65 kW, and an outer stator diameter of 378 mm. In this case, the drivetrain consists of only one machine.

The general simulation methodology for the utilization of different lamination materials is derived from [1] and a description on the numerical modeling given in [14] and [15]. A simple vehicle model for the longitudinal dynamics of a fully electric car is used to study the interdependency of different material utilization in various driving cycles. The power needed in the driving cycle $P_{\mathrm{Cycle(t)}}$ can be calculated with the following equation [16], [17]:

$$P_{\mathrm{Cycle}}(t) = \big(F_{\mathrm{Roll}}(t) + F_{\mathrm{Air}}(t) + F_{\mathrm{Slope}}(t) + F_{\mathrm{Acc}}(t)\big)v(t). \quad (1)$$

The forces in the tread of the tire for the rolling friction F_{Roll}, the air friction F_{Air}, the slope F_{Slope}, and the acceleration F_{Acc} are determined based on the formula introduced in [16], [17]

$$F_{\mathrm{Roll}} = f_r \cdot (m_{\mathrm{vehicle}} + m_{\mathrm{load}}) \cos(\varphi) \quad (2)$$

$$F_{\mathrm{Air}}(t) = \frac{1}{2}\rho_{\mathrm{Air}} c_W A_{\mathrm{vehicle}} v(t)^2 \quad (3)$$

$$F_{\mathrm{Slope}} = (m_{\mathrm{vehicle}} + m_{\mathrm{load}}) \sin(\varphi) \quad (4)$$

$$F_{\mathrm{Acc}} = (m_{\mathrm{vehicle}} e_i + m_{\mathrm{load}}) \frac{dv(t)}{dt} \quad (5)$$

where $v(t)$ is the vehicle's velocity. As the driving cycles do not include information on the altitude profile, φ is set to zero. For each motor topology, a suitable vehicle is chosen. Both vehicles are full electric cars corresponding to actual applications. A summary of the parameters of the vehicle model is given in Table II.

C. Loss Modeling

This study aims to link the structural material parameters and the operational characteristics of electrical machines by using a semiphysical loss description. Both loss modeling approaches, for the IM and for the PMSM, are based on Bertotti's approach [18], [19]. Due to the separation in hysteresis, classical Foucault, and excess losses, a physical interpretation can be enabled, and their sensitivity to the structural parameters can be studied. In the case of the PMSM, the enhanced IEM formula (6) is applied

$$P_{\mathrm{IEM}} = a_1 \hat{B}^{\alpha+\hat{B}\beta} f + a_2 \hat{B}^2 f^2 \left(1 + a_3 \hat{B}^{a_4}\right) + a_5 \left(\hat{B} f\right)^{1.5} \quad (6)$$

where a_1–a_5, α, and β are loss parameters, f is the magnetizing frequency, and $\hat{B}$ is the peak magnetic flux density. The semiphysical parameter identification is described in [20]. The IEM formula is based on the concept of loss separation with the addition of an additional term called the nonlinear losses to account for nonlinear material behavior [20], especially at high frequencies and magnetic flux densities. For the IM, the following model is used:

$$P_{\mathrm{Bertotti}} = k_{\mathrm{hyst}} \hat{B}^{\alpha} f + k_{\mathrm{cl}} \hat{B}^2 f^2 + k_{\mathrm{exc}} \left(\hat{B} f\right)^{1.5} \quad (7)$$

with k_{hyst}, k_{cl}, and k_{exc} being the identified loss parameters. The IM loss modeling is described in [21]. Due to high frequencies of the slotting harmonics and very small frequencies of the rotor current, the iron-loss calculation in the frequency domain for the IM leads to a high computational effort [22]. To avoid this high numerical cost, the iron-loss simulation for the IM is performed in the time domain instead of the frequency domain. According to [15], the transient formulation of the hysteresis losses $p_{\mathrm{hyst}}(t)$, the macroscopic Foucault eddy current losses $p_{\mathrm{cl}}(t)$, and the microscopic excess losses $p_{\mathrm{exc}}(t)$ are added up to represent the iron-loss density $p_{\mathrm{Iron}}(t)$. The total iron losses are then calculated by the temporal mean of the iron-loss density $p_{\mathrm{Iron}}(t)$.

D. Driving Cycles

Driving cycles comprise information on the velocity and acceleration for typical realistic drive scenarios. Further characteristics of driving cycles include the overall time, maximum speed, or maximum acceleration. In the case of this study, the Hyzem cycles and Worldwide harmonized Light Duty Test Cycle (WLTC-3) are chosen. They represent particularly different application fields for full EVs. The operating points of the vehicle are calculated through the vehicle simulation with the driving cycle as input. The electrical speed n is calculated from the vehicle velocity, and the electrical torque

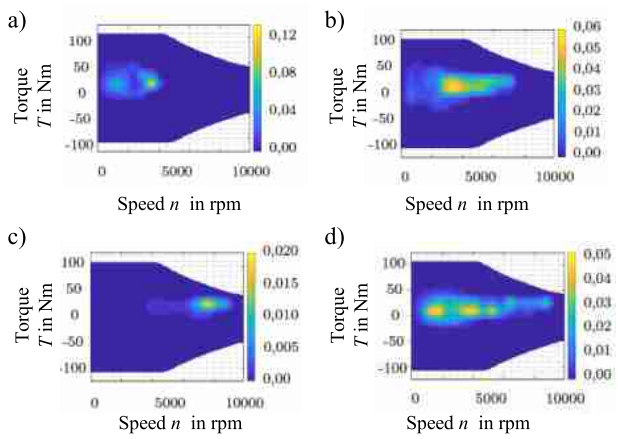

Fig. 1. Operating point distribution share (color bar) in the four driving cycles. (a) Hyzem urban. (b) Hyzem rural. (c) Hyzem highway. (d) WLTC-3.

T is obtained at every given velocity from the force tread of the tire. The operating and probability distribution in the torque–speed map is given in Fig. 1 and shows with which frequency of occurrence certain operating points are present in various driving cycles. There is a distinct difference in the operating point distribution for different driving situations. The urban driving cycle is characterized by low speed and medium torque and represents driving scenarios in cities, where stop-and-go and lower speed limits can be found, whereas the highway driving cycle consists of operating points with high speed. The rural driving cycle WLTC-3 is characterized by a more diverse operating point distribution at high speed and low speed.

III. Results

This work contributes to the deeper understanding of the material and its effect on the electrical machine behavior, highlighting the benefit of tailored material design or appropriate material selection for a specific application to account for different drive scenarios. In the case of speed-variable electrical machines, such as traction drives, the application requirements are specified in the best way by driving cycles instead of single-operation points or an entire torque–speed map. As a result, the ideal material choice relies on specific application requirements.

A. Correlation of Structural Parameters and Loss Components

In Fig. 2, the loss parameters of (6) and (7), that is, the PMSM loss modeling and IM loss modeling, respectively, are shown as a function of different structural parameters. The results indicate that the sheet thickness and grain size are the dominant influences on loss components and thereby most important for material choice or material design.

Due to the identification of hysteresis loss in (6) and (7) from quasi-static or low-frequency measurements, k_{hyst} and a_1 correspond [see Fig. 2(a)]. Both, k_{hyst} and a_1, generally decrease with increasing grain size. This is in accordance with various previous researches on the effect of grain size on hysteresis loss [9], [15]. The materials, however, vary in not only grain size but also the other parameters, such as sheet thickness and alloying. The differences between the materials

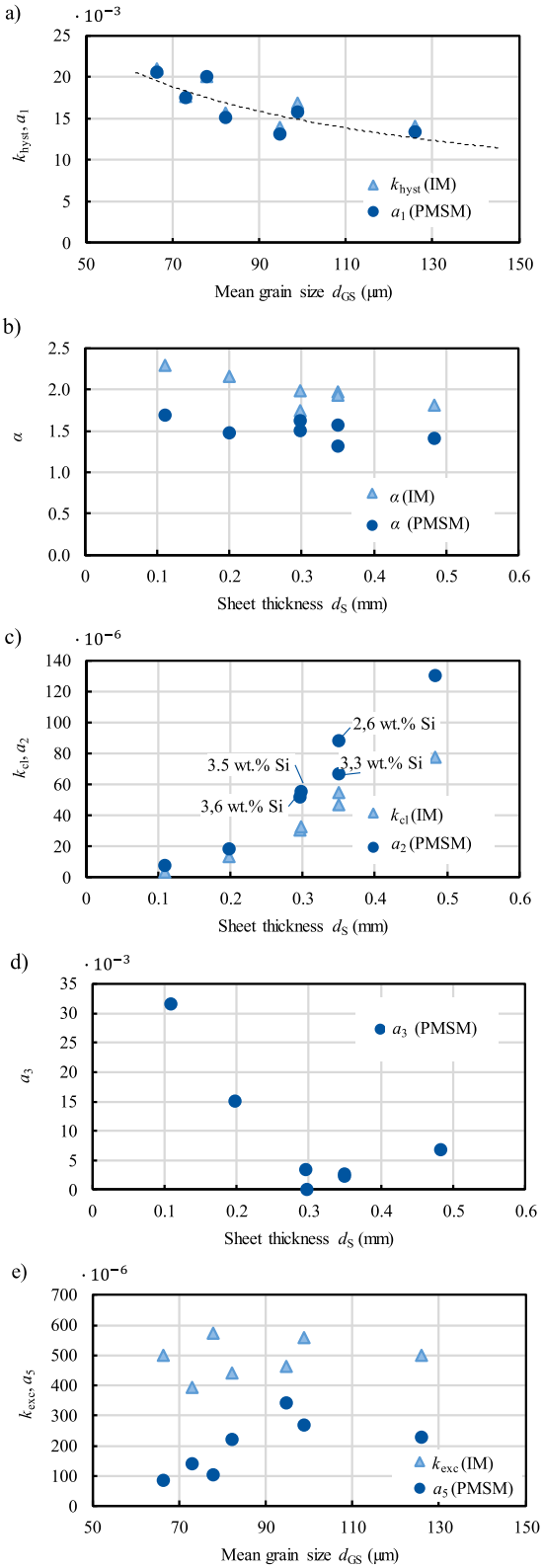

Fig. 2. Structural parameters versus loss parameters for the Bertotti's approach (IM) and the IEM formula (PMSM). (a) Hysteresis-loss parameter vs grain size. (b) Alpha vs. sheet thickness. (c) Foucault Eddy current loss component vs. sheet thickness. (d) Non-linear component vs. sheet thickness. (e) Excess-loss component vs. grain size.

can be further explained. These minor influences also affect the hysteresis loss as summarized in [15]. The exponent of the hysteresis loss α also shows a similar trend for both

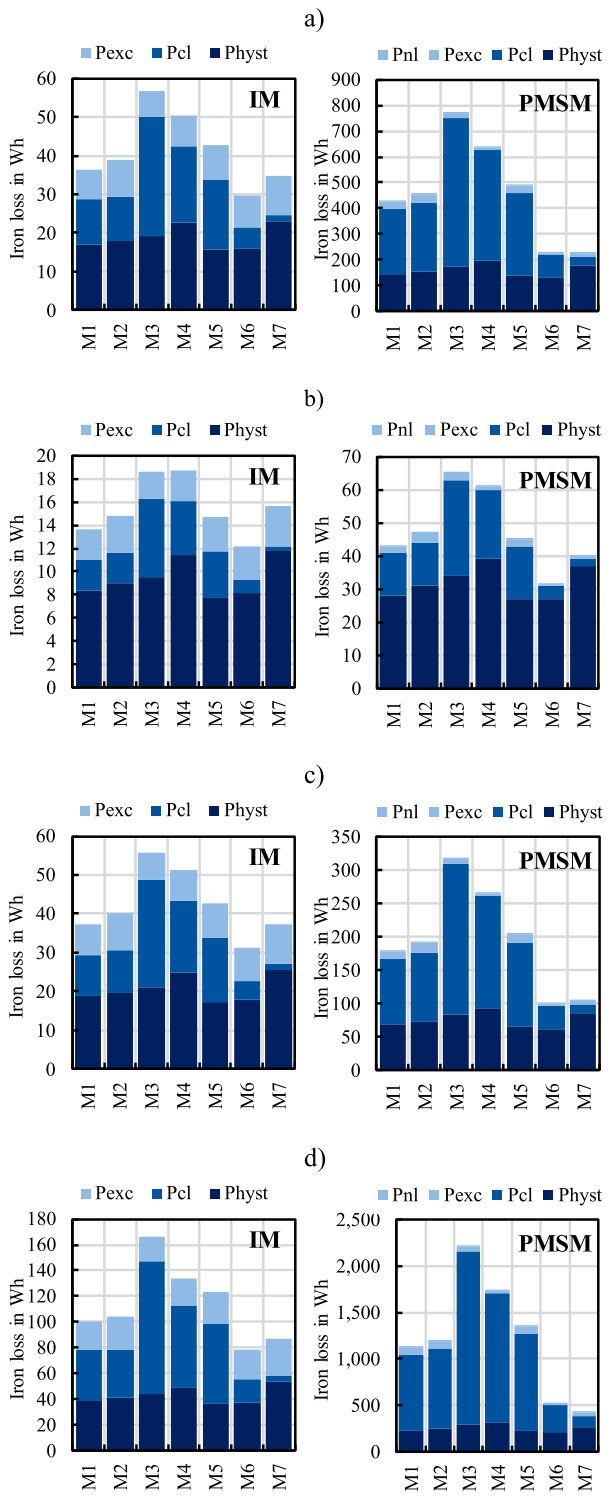

Fig. 3. Results for the iron-loss component distribution in different driving cycles for the studied IM and PMSM for all seven materials. (a) WLTC-3. (b) Hyzem urban. (c) Hyzem rural. (d) Hyzem highway.

modeling approaches; it decreases with the sheet thickness [see Fig. 2(b)]. The difference between the models is the consideration of an additional parameter in the IEM formula. The parameter β depicts a magnetic flux density induction dependence of the exponent. Nevertheless, this additional parameter does not affect the observed trend.

TABLE II
PARAMETERS OF THE VEHICLE MODEL

Specification	Value	PMSM	IM
Vehicle mass	m_{vehicle} in kg	1154	900
Additional mass	m_{load} in kg	160	100
Area vehicle	A_{vehicle} in m²	2.1	2.0
Friction coefficient	f_{r}	0.01	0.01
Air friction coefficient	c_{w}	0.308	0.3
Acceleration coefficient	e_{i}	1.045	1.004

The second loss component, the classical Foucault loss, has a dominant dependence on the sheet thickness due to the analytical calculation method and is proportional to d_{s}^2 [see Fig. 2(c)]. In the case of materials of the same thickness, the silicon content becomes more relevant, as indicated in Fig. 2(c) for the 0.3 and 0.35 mm steel grades. The higher the content is, the lower the classical Foucault losses. Contrary to the thickness, however, alloying seems less important.

The nonlinear losses show no distinct relation to any of the structural parameters. A slight dependence on the sheet thickness can be observed [see Fig. 2(d)], but the results would need to be confirmed with a further study on further materials. The justification of this loss component becomes evident, when the behavior of the excess loss is studied. In the scientific literature [23], the dependence of excess loss on grain size is opposite when compared to the hysteresis loss. Without consideration of the nonlinear component, no distinct grain size dependence can be seen for Bertotti's approach (IM model) but for the IEM formula [see Fig. 2(e)]. One exception can also be observed for the IEM formula (PMSM model), which is the thinnest material. This may give reasons to identify a sheet thickness dependence of excess loss. However, this will have to be studied and confirmed by measurements on further thin materials.

B. Evaluation of Driving-Cycle-Dependent Iron-Loss Component Distribution

In this section, the iron losses of different driving cycles are evaluated for both machine applications, four driving cycles, and all seven materials. The quantitative results are different for both machines, due to different vehicle applications and machine topologies. In order to compare the loss component distributions for the IM and PMSM, the excess and nonlinear losses are summarized in the PMSM evaluation. The results are displayed in Fig. 3.

For the WLTC-3, the best material depends on the machine topology. For the IM, material M6 has the lowest overall losses, whereas for the PMSM, it is M7. In both machines, M3 exhibits the highest overall losses. The hysteresis loss component has a distinctly higher share on total iron loss for the IM compared to the PMSM. M6, that is, the favorable material for the IM, has neither the lowest hysteresis nor the lowest excess or classical losses but due to the combination of structural parameters, the overall lowest iron losses with a sheet thickness of 0.2 mm and a grain size of 95 μm. For the PMSM, the thinnest material has the lowest loss, although the grain size and, thus, the hysteresis loss are higher compared with M6.

The behavior in the urban driving cycle shows that M6 is the best material for this scenario for both machines, due to the low hysteresis and eddy current loss. In this driving cycle, M4 is the worst material for the IM. The classical Foucault losses and sheet thickness are less important, due to the dominance of the hysteresis loss. M3 has not only a distinctly higher thickness but also a lower hysteresis loss compared to M4. For the PMSM, the classical Foucault losses have generally a higher share so that M4 has lower losses compared to M3.

In the rural driving scenario, the trend for the IM and PMSM is similar for all studied materials M3 > M4 > M5 > M2 > M1 > M7 > M6. In the highway cycle, a similar behavior as for the WLTC can be observed. Especially, for the PMSM, the classical Foucault loss is dominant and, thus, the sheet thickness becomes the most important structural parameter.

M1 and M2 are generally very similar materials, with similar thickness, grain size, and silicon content. Although M1 has smaller grains, it has slightly smaller hysteresis loss. This can be due to the measurement of grain size or additional effects of sheet thickness, residual stress, or impurities.

In general, it can be denoted that the machine topology and driving cycles need to be considered for the material choice. The combination of structural material parameters affects the iron-loss distribution. The highest classified grades do not necessarily lead to the smallest overall losses. Furthermore, the copper losses also vary for different applications, which have to be considered for the overall efficiency as well.

IV. Conclusion

This work contributes to the deep understanding of the ferromagnetic material and its effect on electrical machine behavior.

With a deeper understanding of the correlation between structural and iron-loss parameters, the magnetic properties of a given electrical steel can be estimated from its material parameters instead of magnetic measurements. For example, a material with a grain size of 110 μm [see Fig. 2(a)] likely has lower hysteresis, that is, low-frequency losses than most of the respective studied materials. This approach stems from the problem that magnetic measurements are performed at discrete frequencies. With a loss model parameter correlation, any frequency can be extrapolated beyond and in between these discrete measurements.

The results of the simulation study further show that the application requirements have to be considered for the best possible material choice. The structural parameters reflect in the iron-loss distribution more than the general classification. This highlights the benefit of tailored material design or material parameter-dependent choice of material.

1) In the case of speed–variable machines, such as traction drives, the application requirements are in the best way specified by employing drive cycles instead of single-operation points or an entire torque–speed map.
2) Structural parameters affect the loss parameters of semi-physical loss models. Grain size and sheet thickness are dominant parameters.
3) The ideal material is dependent on the machine topology and driving cycle and is not necessarily correlated with the highest grade considering the standardized classification of iron losses per weight at 1.5 T and 50 Hz magnetization frequency.
4) In this study, the overall best suitable material for various driving cycles and both machines' lamination had a thickness of 0.2 mm and a grain size of 95 μm, neither the thinnest material nor the one with the largest or the smallest grain size.

The presented results show that for certain applications, an appropriate material choice can improve the performance data of a drivetrain. In the highway driving cycle, for example, the sheet thickness is most important. The addition of higher silicon content is not necessary, as it hampers the production of thin sheet. Furthermore, the grain size can be chosen smaller, as the hysteresis loss is less dominant in this cycle. Smaller grains can be achieved by less heat during annealing in the material's production process. In the urban driving cycle on the other hand, higher sheet thickness can be beneficial, because first, the classical Foucault loss is less dominant and second, grain growth is less limited across the sheet thickness and high grain size leads to lower hysteresis loss.

Acknowledgment

This work was supported by the Deutsche Forschungsgemeinschaft (DFG) through the Research Group Project "For 1897-Low-Loss Electrical Steel for Energy-Efficient Electrical Drives" under Grant 255713208.

References

[1] A. Ruf, S. Steentjes, G. von Pfingsten, T. Grosse, and K. Hameyer, "Requirements on soft magnetic materials for electric traction motors," in *Proc. 7th Int. Conf. Magn. Metall. (WMM)*, vol. 2016, pp. 111–128.
[2] A. Krings, A. Boglietti, A. Cavagnino, and S. Sprague, "Soft magnetic material status and trends in electric machines," *IEEE Trans. Ind. Electron.*, vol. 64, no. 3, pp. 2405–2414, Mar. 2017.
[3] F. J. G. Landgraf, "Nonoriented electrical steels," *JOM*, vol. 64, no. 7, pp. 764–771, Jul. 2012.
[4] A. J. Moses, "Energy efficient electrical steels: Magnetic performance prediction and optimization," *Scripta Mater.*, vol. 67, no. 6, pp. 560–565, Sep. 2012.
[5] Y. Oda, M. Kohno, and A. Honda, "Recent development of non-oriented electrical steel sheet for automobile electrical devices," *J. Magn. Magn. Mater.*, vol. 320, no. 20, pp. 2430–2435, Oct. 2008.
[6] D. C. Jiles, *Introduction to Magnetism and Magnetic Materials*, 3rd ed. Boca Raton, FL, USA: CRC Press, 2016.
[7] K. M. Krishnan, *Fundamentals and Applications of Magnetic Materials*. New York, NY, USA: Oxford Univ. Press, 2016.
[8] C. Chen, *Magnetism and Metallurgy of Soft Magnetic Materials*. New York, NY, USA: Dover, 1986.
[9] M. F. de Campos, J. C. Teixeira, and F. J. G. Landgraf, "The optimum grain size for minimizing energy losses in iron," *J. Magn. Magn. Mater.*, vol. 301, no. 1, pp. 94–99, 2006.
[10] R. M. Bozorth, *Ferromagnetism*. New York, NY, USA: Van Nostrand, 1951.
[11] L. Kestens and S. Jacobs, "Texture control during the manufacturing of nonoriented electrical steels," *Texture, Stress, Microstruct.*, vol. 2008, pp. 1–9, 2008.
[12] N. Leuning, S. Steentjes, M. Heller, S. Korte-Kerzel, and K. Hameyer, "On the correlation of crystallographic macro-texture and magnetic magnetization anisotropy in non-oriented electrical steel," *J. Magn. Magn. Mater.*, vol. 490, Nov. 2019, Art. no. 165485.
[13] *Magnetic materials-Part 13: Methods of measurement of density, resistivity and stacking factor of electrical steel sheet and strip*, document (IEC 60404-13:1995); German version EN 60404-13, 2007.
[14] N. Leuning, S. Elfgen, B. Groschup, G. Bavendiek, S. Steentjes, and K. Hameyer, "Advanced soft- and hard-magnetic material models for the numerical simulation of electrical machines," *IEEE Trans. Magn.*, vol. 54, no. 11, pp. 1–8, Nov. 2018.

[15] M. Nell, N. Leuning, S. Mönninghoff, and B. Groschup, "Complete and accurate modular numerical computation scheme for multi-coupled electric drive systems," *IET Sci., Meas. Technol.*, vol. 14, no. 3, pp. 259–271, 2020.
[16] L. Eckstein, *Langsdynamik von Kraftfahrzeugen-Verkehrssystem Kraftfahrzeug, Vorlesungsumdruck Fahrzeugtechnik I Zitieren*, 4th ed. Aachen, Germany, 2011.
[17] J. C. Maxwell, *A Treatise on Electricity and Magnetism*, vol. 2, 3rd ed. Oxford, U.K.: Clarendon, 1892, pp. 68–73.
[18] G. Bertotti, *Hysteresis in Magnetism: For Physicists, Materials Scientists, and Engineers*. New York, NY, USA: Academic, 1998.
[19] G. Bertotti, "General properties of power losses in soft ferromagnetic materials," *IEEE Trans. Magn.*, vol. 24, no. 1, pp. 621–630, Jan. 1988.
[20] S. Steentjes, M. Leßmann, and K. Hameyer, "Semi-physical parameter identification for an iron-loss formula allowing loss-separation," *J. Appl. Phys.*, vol. 113, no. 17, May 2013, Art. no. 17A319.
[21] G. von Pfingsten, "The induction machine as speed variable drive for automotive traction applications," Ph.D. dissertation, IEM RWTH Aachen University, Shaker Verlag, Aachen, Germany, 2018, p. 200.
[22] M. Nell, N. Leuning, S. Mönninghoff, and B. Groschup, "Complete and accurate modular numerical computation scheme for multi-coupled electric drive systems," *IET Sci., Meas. Technol.*, vol. 14, no. 3, pp. 259–271, 2019.
[23] DieselNet. (2006). *Summary of worldwide engine and vehicle test cycles*. [Online]. Available: http://www.dieselnet.com/standars/cycles#eu
[24] F. J. G. Landgraf, M. Emura, J. C. Teixeira, and M. F. de Campos, "Effect of grain size, deformation, aging and anisotropy on hysteresis loss of electrical steels," *J. Magn. Magn. Mater.*, vols. 215–216, pp. 97–99, Jun. 2000.
[25] A. Krings and J. Soulard, "Overview and comparison of iron loss models for electrical machines," *J. Elect. Eng.*, vol. 10, no. 3, pp. 162–169, 2010.
[26] G. Bertotti, "Connection between microstructure and magnetic properties of soft magnetic materials," *J. Magn. Magn. Mater.*, vol. 320, no. 20, pp. 2436–2442, Oct. 2008.